The Astrophysical Journal, 711:980–989, 2010 March 10 doi:10.1088/0004-637X/711/2/980

DROPOUTS IN SOLAR ENERGETIC PARTICLES: ASSOCIATED WITH LOCAL TRAPPING BOUNDARIES OR CURRENT SHEETS?

A. Seripienlert[1,2], D. Ruffolo[1,2], W. H. Matthaeus[3], and P. Chuychai[2,4]
[1] Department of Physics, Faculty of Science, Mahidol University, Bangkok 10400, Thailand; achara.seri@gmail.com, scdjr@mahidol.ac.th
[2] ThEP Center, CHE, 328 Si Ayutthaya Road, Bangkok 10400, Thailand
[3] Bartol Research Institute and Department of Physics and Astronomy, University of Delaware, Newark, DE 19716, USA; yswhm@bartol.udel.edu
[4] School of Science, Mae Fah Luang University, Chiang Rai 57100, Thailand; piyanate@gmail.com
Received 2009 November 13; accepted 2010 January 27; published 2010 February 19

ABSTRACT

In recent observations by the *Advanced Composition Explorer*, the intensity of solar energetic particles exhibits sudden, large changes known as dropouts. These have been explained in terms of turbulence or a flux tube structure in the solar wind. Dropouts are believed to indicate filamentary magnetic connection to a localized particle source near the solar surface, and computer simulations of a random-phase model of magnetic turbulence have indicated a spatial association between dropout features and local trapping boundaries (LTBs) defined for a two-dimensional (2D) + slab model of turbulence. Previous observations have shown that dropout features are not well associated with sharp magnetic field changes, as might be expected in the flux tube model. Random-phase turbulence models do not properly treat sharp changes in the magnetic field, such as current sheets, and thus cannot be tested in this way. Here, we explore the properties of a more realistic magnetohydrodynamic (MHD) turbulence model (2D MHD), in which current sheets develop and the current and magnetic field have characteristic non-Gaussian statistical properties. For this model, computer simulations that trace field lines to determine magnetic connection from a localized particle source indicate that sharp particle gradients should frequently be associated with LTBs, sometimes with strong 2D magnetic fluctuations, and infrequently with current sheets. Thus, the 2D MHD + slab model of turbulent fluctuations includes some realistic features of the flux tube view and is consistent with the lack of an observed association between dropouts and intense magnetic fields or currents.

Key words: interplanetary medium – magnetic fields – magnetohydrodynamics (MHD) – Sun: particle emission – turbulence

1. INTRODUCTION

Observations of the interplanetary medium, and in particular the solar wind and magnetic fields evolving from their solar source, have revealed a complex spatial and temporal structure in plasma and magnetic properties. In addition to large-scale discontinuities such as corotating interaction regions, coronal mass ejections, and their associated shocks, as well as magnetic sector boundaries, there is also strong evidence for small-scale structure and filamentary connection to the Sun. Such evidence includes strong tails in statistical distributions of changes in magnetic field direction and plasma properties (e.g., Bruno et al. 2001; Borovsky 2008; Li 2008; Greco et al. 2009). In addition, particularly useful probes of magnetic connection are solar energetic particles (SEPs) from impulsive solar flares. Such flares occur as discrete events and inject particles from a small region of the solar surface (Reames et al. 1990), and SEPs of energies $\lesssim$10 MeV follow magnetic field lines quite closely, so the particles serve as excellent tracers of magnetic connection from a localized particle source at the Sun. The "dropouts" in SEPs from impulsive solar flares (Mazur et al. 2000; Gosling et al. 2004), in which the measured particle flux undergoes sudden, large changes, frequently seeming to disappear and reappear, suggest a filamentary distribution of magnetic connection to the particle source (Giacalone et al. 2000; Ruffolo et al. 2003; Zimbardo et al. 2004).

One interpretation of the filamentary connection to the Sun is that the solar wind comprises "spaghetti-like" winding flux tubes separated by sharp boundaries (Parker 1963b; McCracken & Ness 1966; Bruno et al. 2001; Borovsky 2008). In this view, the flux tube boundaries are taken to be distinct from the well-known magnetic fluctuations with a turbulent power spectrum (Jokipii & Coleman 1968). From another point of view, the apparent flux tube structure could be a natural consequence of the turbulent evolution of magnetic fluctuations in a plasma. Starting from fluctuations in the magnetic field at the solar wind source, the larger-scale structures evolve more slowly (Kármán & Howarth 1938; Matthaeus et al. 1996), and could survive as "fossil turbulence" at a distance of 1 AU from the Sun (Giacalone et al. 2006), while smaller-scale structures join a turbulent cascade (Kolmogorov 1941) to even smaller scales where the energy is dissipated (Coleman 1968; Verma et al. 1995; Leamon et al. 1998; Sahraoui et al. 2009). A number of studies (Matthaeus et al. 1990; Bieber et al. 1996) have observed that interplanetary magnetic fluctuations near Earth necessarily include wavevectors **k** that are parallel ("slab" fluctuations) and perpendicular ("2D" fluctuations) to the large-scale field, with less power at oblique wavevectors. It has been proposed that the interaction of counter-propagating fluctuations with a component of **k** parallel to the mean field can naturally produce 2D fluctuations at much higher perpendicular **k**, leading to a component that can become approximately 2D. MHD simulations have provided substantial evidence for this (Shebalin et al. 1983; Oughton et al. 1994), and various models (Montgomery 1982; Higdon 1984; Goldreich & Sridhar 1995) build in this anisotropy as an assumption. A 2D-like component can account for most of the interplanetary magnetic fluctuation energy (Bieber et al. 1996), and is very similar to the reduced MHD model (Strauss 1976; Montgomery 1982; Zank & Matthaeus 1991). These processes naturally produce a flux-tube like structure, yet allow the possibility that slab fluctuations "shred" or distort the flux surfaces (Matthaeus et al. 1995; Ruffolo et al. 2004). The simple model that we employ below is a parameterization that represents most of these properties.

Based on theoretical results that express the magnetic field line diffusion coefficient in terms of the turbulent power spectrum (Jokipii & Parker 1968; Matthaeus et al. 1995), it is a reasonable first step to model turbulent fluctuations by summing over Fourier modes with the appropriate power spectrum and to simply assign a random phase to each wave mode. Indeed, models of magnetic turbulence frozen-in from the solar source (Giacalone et al. 2000), with two components of slab and 2D fluctuations (Ruffolo et al. 2003; Chuychai et al. 2007), and with three-dimensional fluctuations (Zimbardo et al. 2004; Pommois et al. 2005) have all been able to generate filamentary magnetic connection that explain dropouts.

Given that large-scale diffusion of SEPs is quite rapid (McKibben et al. 2001; McKibben 2005), specific mechanisms are needed to explain sharp particle gradients over intermediate distance scales. In the turbulence view, proposed mechanisms include temporary topological trapping of field lines in "islands" of the 2D turbulence (Ruffolo et al. 2003) and suppressed diffusive escape where the 2D field is strong or irregular (Chuychai et al. 2005, 2007; Tooprakai et al. 2007). Over a long distance scale, magnetic field lines can escape their temporary topological traps and undergo rapid lateral diffusion. Naturally, the question arises as to the boundary of the "islands" of field line trapping. In simulation results for random-phase 2D+slab turbulence, Chuychai et al. (2007) identified local trapping boundaries (LTBs), defined as contours of constant 2D potential where $|b^{2D}|^2_{av}$ is maximized with respect to neighboring contours, as frequently defining sharp changes in magnetic connection where dropout features would be expected, which in some cases can be interpreted as boundaries of trapping regions. The LTBs reflect the concept of temporary trapping along closed 2D orbits, with eventual escape due to slab fluctuations, as well as the suppression of slab diffusive escape where the 2D field is strong. Note that the turbulence is homogeneous, and there is no "input" structure; the "islands" are regions around local maxima and minima of a random 2D potential function.

The distinctions between the flux tube view and the turbulence view are sometimes not recognized. For example, in the context of observationally testing the concepts developed from turbulence models, Chollet & Giacalone (2008) pointed out that dropout features are not well correlated with sharp magnetic field changes (such as current sheets). However, that observation actually addresses the flux tube view, in which trapping within flux tubes is naturally envisioned as delineated by magnetic field changes, whereas simulations of random-phase turbulence had indicated trapping within LTBs. In general, the lack of an observed association between dropouts and features of the magnetic field or current (Mazur et al. 2000; Gosling et al. 2004; Chollet & Giacalone 2008) is problematic for the flux tube view, in which the only surfaces available to trap plasma and field lines are, by assumption, the flux tube boundaries themselves.

Another concern is the space filling of the field line trapping regions (Kaghashvili et al. 2006), because a high space filling could inhibit the transport of particles perpendicular to the mean magnetic field. In the random-phase 2D+slab model, the 2D "islands" of temporary field line trapping are delineated by LTBs, yielding a moderate space filling (Chuychai et al. 2007). Field lines in the interstitial "network" can rapidly diffuse perpendicular to the mean field (Ruffolo et al. 2003). This result is consistent with observations of SEP from impulsive solar events. Flux-limited surveys, which require a substantial particle intensity, indicate a narrow distribution for such events in solar longitude (Reames 1992). This indicates only limited lateral spreading for the bulk of SEPs, which we attribute to trapping within small-scale topological islands, representing a "core" region of high particle density (see Figure 3 of Ruffolo et al. 2003). At the same time, observations of type III radio bursts, which are sensitive to very low particle fluxes, indicate that SEPs can undergo lateral motion by up to $\sim 90^\circ$ in solar longitude during their transport from the Sun to Earth orbit (Cane & Erickson 2003). This laterally extended but less intense "halo" of SEPs corresponds to particles on field lines initially located in interstitial regions between the 2D islands. Indeed, the absence of these halo SEPs from the core region is manifest as dropouts.

In contrast, descriptions of the flux tube viewpoint typically propose space-filling trapping regions, sometimes with a strict interpretation of field line confinement in the flux tubes (see Figure 1 and Section 8.1 of Borovsky 2008). Even if one invokes a "cross-field" diffusion mechanism whereby particles can cross field lines, it is difficult to reconcile escape that is slow enough to preserve dropout features with the rapid diffusion of SEPs as inferred from observations over short timescales (Cane & Erickson 2003) and long timescales (McKibben et al. 2001; McKibben 2005), as well as the important role played by perpendicular diffusion in the solar cycle dependent modulation of Galactic cosmic rays (Parker 1965; Moraal 1976; Cane et al. 1999; Reinecke et al. 2000).

On the other hand, random-phase models of turbulence do not contain current sheets, i.e., strong, thin current structures, which clearly are present in the interplanetary medium. Current sheets, or discontinuous or sharp magnetic features in general, require that a large number of Fourier modes have coordinated phases to create a jump that is spatially localized. The correlations required to establish these structures are generated rapidly by nonlinear turbulence processes (Servidio et al. 2008) that are associated with non-Gaussian statistics and intermittency (Wan et al. 2009). Random-phase models are also unable to explain the observed distributions of strong jumps in various properties of the solar wind as presented by Borovsky (2008).

In the present work, we aim to rectify these shortcomings in the turbulence models by replacing the 2D random-phase field by the output of a 2D MHD simulation. While computationally time-consuming, a 2D MHD model incorporates the microphysics of the plasma to produce current sheets and structures resembling flux tubes. In this way, the concepts of the flux tube view naturally appear in a more physical model of the turbulent magnetic field. A 2D MHD + slab field with filamentary magnetic connection has previously been used in an explanation of "moss" emission in the solar transition region (Kittinaradorn et al. 2009). Here, we examine the general properties of the 2D MHD field, in comparison with the random-phase field, and trace magnetic field lines in a 2D MHD+slab field in order to examine the expected dropout features of SEPs from impulsive solar flares. We find that dropout features, i.e., sharp changes in magnetic connection to a localized source, are frequently associated with LTBs, are sometimes associated with strong 2D magnetic fluctuations, and are only infrequently associated with current sheets. Thus, a more realistic model of turbulent fluctuations can incorporate some attractive features of the flux tube view and is consistent with the lack of an observed association between dropouts and intense magnetic fields or currents.

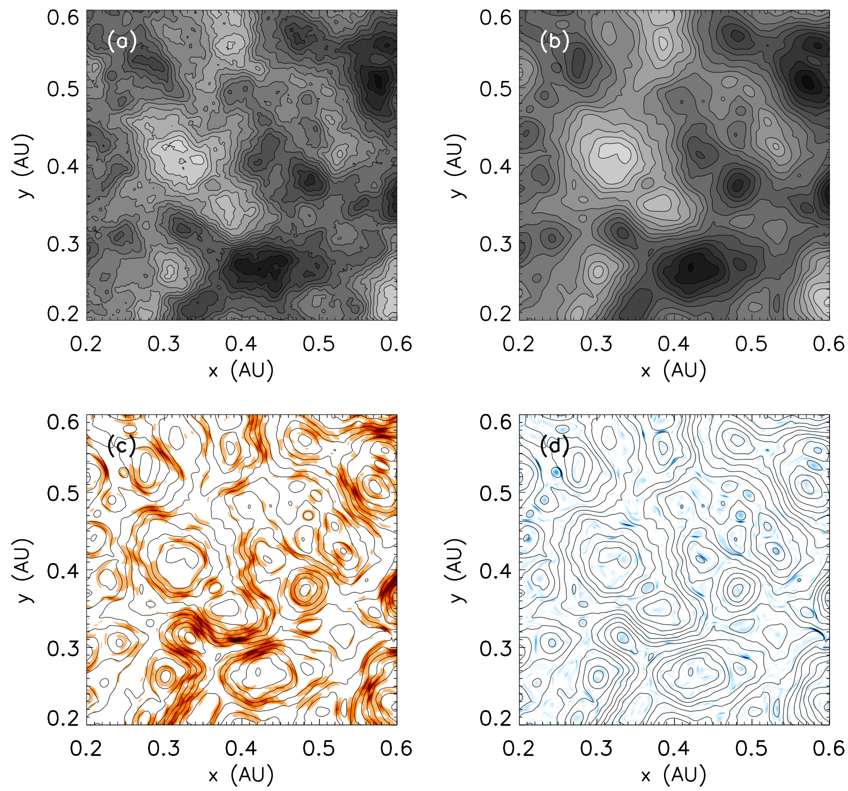

Figure 1. 2D component of magnetic turbulence can be defined in terms of an irregular potential function $a(x, y)$, whose curl is $\mathbf{b}^{2D}$. We compare contours of constant potential, i.e., magnetic flux surfaces, for (a) a 2D random-phase field, in which a is a random function with a turbulent power spectrum and (b) the same field after a 2D MHD procedure. A darker shading indicates a higher value of a. For the 2D MHD field, the contours of constant potential are superimposed with coloring to indicate (c) b^2 and (d) j^2, for a current $\mathbf{j} = \nabla \times \mathbf{b}$. The 2D MHD field is a more physically realistic model, reproducing aspects of the flux tube viewpoint, but with the current concentrated in narrow current sheets. The present work examines the level of association between b^2 or j^2 and sharp changes in field line connection over a distance of 1 AU, which relates to dropouts (sharp density changes) in SEPs as observed near Earth.

2. MAGNETIC TURBULENCE MODELS AND SIMULATION TECHNIQUES

2.1. 2D + Slab Model

In this work, we express the interplanetary magnetic field as

$$\boldsymbol{B} = B_0\hat{\mathbf{z}} + \mathbf{b}(\boldsymbol{x}, \boldsymbol{y}, z), \tag{1}$$

where $B_0\hat{\mathbf{z}}$ is a constant mean field and $\mathbf{b}$ is the transverse fluctuating part, which can be separated into two components, a "slab" component that depends only on the z coordinate and a "2D" component that depends only on the x and y coordinates. Thus, $\mathbf{b}$ can be written as

$$\boldsymbol{b}(\boldsymbol{x}, \boldsymbol{y}, z) = \mathbf{b}^{\mathrm{slab}}(z) + \mathbf{b}^{\mathrm{2D}}(\boldsymbol{x}, \boldsymbol{y}). \tag{2}$$

Because $\nabla \cdot \boldsymbol{B} = 0$, we have $\nabla \cdot \mathbf{b}^{2D} = 0$ and $\mathbf{b}^{2D} = \nabla \times [a(x, y)\hat{\mathbf{z}}]$ for a scalar potential function $a(x,y)$. If there were only 2D fluctuations, the magnetic field lines would exactly follow 2D flux surfaces defined by contours of constant potential, but the addition of the slab component allows field lines to diffuse away from the 2D flux surfaces.

This magnetic field model was motivated by the work of Matthaeus et al. (1990), who found that the fluctuation power of the solar wind is concentrated at wavevectors nearly perpendicular and parallel to the mean magnetic field (see also Dasso et al. 2005; Weygand et al. 2009). In addition to its use in the study of dropouts, the two-component model has also provided a useful description of solar wind fluctuations (Bieber et al. 1996; Saur & Bieber 1999; Osman & Horbury 2007) and the parallel transport of particles in interplanetary space (Bieber et al. 1994; Shalchi et al. 2008). In our simulations, we set the root mean square fluctuating field as $b = 0.5B_0$ and the ratio of slab energy to 2D energy as 20:80 (Bieber et al. 1994, 1996) so that $\langle b^2\rangle^{\mathrm{slab}} = 0.05B_0^2$ and $\langle b^2\rangle^{\mathrm{2D}} = 0.2B_0^2$.

2.2. Random-phase Fields

To numerically generate the fluctuating fields, we require a Kolmogorov power spectrum of turbulence in the inertial region of k-space. For the slab component, we can write

$$P_{xx}^{\mathrm{slab}}(k_z) = P_{yy}^{\mathrm{slab}}(k_z) = \frac{C^{\mathrm{slab}}}{[1 + (k_z\lambda)^2]^{5/6}}, \tag{3}$$

where C^{slab} is a normalization constant and λ is the parallel coherence length, set to 0.02 AU. This spectral form yields a Kolmogorov power law, $k_z^{-5/3}$, in the inertial range at higher k_z, and is independent of k_z in the energy-containing range at lower k_z; such spectra have been found in observations of solar wind fluctuations (Jokipii & Coleman 1968). The magnetic field in the wavevector domain can be written as

$$b_x^{\mathrm{slab}}(k_z) = \sqrt{P_{xx}^{\mathrm{slab}}(k_z)}e^{i\phi_x(k_z)}, \tag{4}$$

where i is $\sqrt{-1}$ and ϕ_x is a random phase that is independent for each Fourier mode, varying from 0 to 2π. For the y-component, we use

$$b_y^{\mathrm{slab}}(k_z) = \sqrt{P_{yy}^{\mathrm{slab}}(k_z)}e^{i\phi_y(k_z)}. \tag{5}$$

Because of the use of random phases ϕ_x and ϕ_y, this can be called a random-phase field.

Then, we use an inverse fast Fourier transform (FFT) to obtain the fluctuating magnetic fields in real space. In our simulations, we set the box length in the z-direction to $L_z = 10{,}000\lambda$, and the number of grid points was $N_z = 4{,}194{,}304$. The field lines are traced only to a few percent of the simulation box length in order to avoid periodic effects. The power spectrum of the random-phase 2D potential is

$$A(k_\perp) = \frac{C^{2D}}{[1 + (k_\perp \ell_\perp)^2]^{7/3}}, \tag{6}$$

where $A(k_\perp)$ is the power spectrum of $a(x, y)$, defined as the Fourier transform of the correlation function $\langle a(\boldsymbol{r}_0)a(\boldsymbol{r}_0 + \mathbf{r})\rangle$, C^{2D} is a normalization constant, $k_\perp = \sqrt{k_x^2 + k_y^2}$, and $\ell_\perp$ is a perpendicular coherence length, set to 0.03 AU (similar to the value used by Ruffolo et al. 2003). This leads to an omnidirectional power spectrum, $\mathcal{E}(k_\perp)$, with a Kolmogorov power law in the inertial range and a $k_\perp^2$ dependence in the energy-containing range as required for homogeneity (Ruffolo et al. 2004; Matthaeus et al. 2007). The magnetic potential for the 2D component in the wavenumber domain is

$$a(k_x, k_y) = \sqrt{A(k_\perp)}e^{i\phi(k_x,k_y)}, \tag{7}$$

where ϕ is a random phase. We derived $b_x^{2D}(\mathbf{k})$ and $b_y^{2D}(\mathbf{k})$, and used the FFT algorithm (Press et al. 1992) to perform the inverse Fourier transform to obtain $\mathbf{b}^{2D}(x, y)$ in the spatial domain box lengths $L_x = L_y = 40\lambda$. The numbers of grid points were $N_x = N_y = 1{,}024$. An example of a 2D random-phase potential function $a(x,y)$ generated in this manner is shown in Figure 1(a).

2.3. 2D MHD Field

Random-phase models of magnetic fields encode the desired power spectrum, e.g., for a turbulent plasma, and since the power spectrum is the Fourier transform of the spatial correlation function, the latter should be correctly treated as well, in the ensemble average. However, random-phase models have some physical deficiencies, especially in two or more dimensions. Therefore, for the 2D magnetic field component, we have developed a procedure for "processing" a random-phase field according to MHD in two dimensions.

According to MHD, the magnetic pressure depends on b^2, so the turbulent flow will tend to make $|\mathbf{b}|$ more uniform. Thus, the current $\mathbf{j}$, which depends on $\nabla \times \mathbf{b}$, is reduced in most locations, but remains at topological "defects" where $\mathbf{b}$ changes in magnitude and/or direction. This topological structure is a key feature of the flux tube viewpoint, and the topology requires current cores in the interior and current sheets at the flux tube boundary (Matthaeus & Lamkin 1986; Greco et al. 2009); these will be discussed further in Section 3.1. Along the flux tube boundary, the attraction of parallel current elements should concentrate such currents into narrow regions, such as current sheets with magnetic reconnection. Thus, the current sheets should be envisioned as not uniformly spread over the flux tube boundary but rather concentrated at narrow portions thereof.

A random-phase 2D field assumes independent Fourier modes and therefore does not incorporate the tendency of $|\mathbf{b}|$ to become more uniform and $|\mathbf{j}|$ to become more concentrated, which require that many Fourier modes "conspire" to concentrate changes in the magnetic field and form coherent current structures in localized regions.

In the solar wind, we expect that an initial fluctuation field, e.g., from the solar source, should undergo substantial MHD evolution before arriving at Earth. The dynamical age of the solar wind at Earth orbit can be roughly estimated from

$$\frac{T}{T_{nl}} = C_{ch}\frac{R/U}{L/Z}, \tag{8}$$

where T is the solar wind travel time from the Sun, T_{nl} is a nonlinear scale time, specifically, the eddy turnover time at the outer scale, $C_{ch} = 0.5$ is a constant to account for cross-helicity (Alfvénic) effects (see Hossain et al. 1996), R is the distance from the Sun, U is the solar wind speed, L is the outer scale of the turbulence, and Z is eddy velocity at the outer scale. Using $R = 1$ AU and observations at 1 AU of $U = 300$–600 km s^{-1}, $L = 0.01$ AU (Weygand et al. 2009), and $Z = 20$–40 km s^{-1} (see Smith et al. 2001 for observations of the normal component of Z^2), it can be estimated that the solar wind experiences ∼2–17 nonlinear scale times on its way to Earth orbit. Because there is continual energy input (e.g., Matthaeus et al. 1998), the solar wind turbulence is fully developed at 1 AU, and the power spectrum is observed to be close to a Kolmogorov form (Jokipii & Coleman 1968).

In the present work, we model such turbulent evolution by starting from an initial random-phase 2D field, which incorporates a turbulent power spectrum. Then, a 2D pseudospectral incompressible MHD code (see Wan et al. 2009) is employed to evolve the magnetic configuration according to the following equations of evolution,

$$\begin{aligned} \frac{\partial \omega}{\partial t} + \mathbf{v} \cdot \nabla\omega &= \mathbf{b} \cdot \nabla j + \nu\nabla^2\omega \\ \frac{\partial a}{\partial t} + \mathbf{v} \cdot \nabla a &= \eta\nabla^2 a, \end{aligned} \tag{9}$$

in terms of the plasma vorticity $\omega = (\nabla \times \mathbf{v}) \cdot \hat{\mathbf{z}}$, plasma velocity $\mathbf{v}$, current $j = (\nabla \times \mathbf{b}) \cdot \hat{\mathbf{z}}$, molecular viscosity ν, and resistivity η. The simulation has 1024×1024 spatial resolution and a magnetic Reynolds number of 640 at the largest scales. Because 2D MHD simulations do not include energy input to the turbulence, and use a lower Reynolds number than solar wind turbulence, their turbulent energy decays more quickly than that in the solar wind. Here, the simulation is run from $t = 0$ to T_{nl}, which is sufficient for developing nonlinear structures (i.e., phase correlations of Fourier components) but not so long as to severely distort the power spectrum away from a Kolmogorov form. At $t \sim T_{nl}$, the decaying turbulence has reached the peak of its dissipation and most closely resembles steady-driven fully developed turbulence as expected in the solar wind. We then obtain the 2D MHD potential, magnetic field, and current.

2.4. Field Line Tracing

After obtaining the magnetic field at each grid point of the simulation box, magnetic field line trajectories were found by solving the coupled equations

$$\frac{dx}{dz} = \frac{b_x^{2D}(x, y) + b_x^{slab}(z)}{B_0}, \quad \frac{dy}{dz} = \frac{b_y^{2D}(x, y) + b_y^{slab}(z)}{B_0} \tag{10}$$

to obtain $x(z)$ and $y(z)$. We solve Equation (10) using a fourth-order Runge–Kutta method with an adaptive step size (Press et al. 1992). The magnetic field at each position is obtained by linear interpolation (slab component) and bilinear interpolation

(2D component). Then, 10,000 field lines from random initial (x, y) locations within a circle of radius 0.1 AU centered at (0.4 AU, 0.4 AU) are traced from $z = 0$, corresponding to the particle source, to a distance of $z = 1$ AU. We then examine the distribution of (x, y) locations, especially the sharp gradients in the density of field lines connected to the source, as an indicator of where dropouts can be observed as the solar-corotating field lines pass the observer. As a check, we have also traced particle trajectories by solving the Newton–Lorentz equations as function of time, using similar techniques (for details, see Tooprakai et al. 2007).

2.5. Local Trapping Boundaries

Previous computer simulations that traced turbulent magnetic field lines, as described above, have found sharp gradients in the density of field lines connected to the source as a function of x and y (Ruffolo et al. 2003; Zimbardo et al. 2004). The proposed physical mechanisms are (1) temporary topological trapping along flux surfaces of constant 2D potential $a(x, y)$, with eventual diffusive escape due to the slab fluctuations (Ruffolo et al. 2003), and (2) suppressed diffusive escape where the 2D field is strong (Chuychai et al. 2005). Combining the two ideas leads to the concept of LTBs, i.e., 2D flux surfaces where the 2D field is particularly strong (Chuychai et al. 2007).

LTBs are contours of constant potential a in the x–y plane whose average 2D fluctuation energy is maximized with respect to neighboring contours, i.e.,

$$\text{Maximize} : |b^{2\mathrm{D}}|^2_{\mathrm{av}} = \frac{1}{L}\oint |b^{2\mathrm{D}}(x, y)|^2 d\ell, \tag{11}$$

where $|b^{2\mathrm{D}}|$ is the local strength of the 2D magnetic field, $d\ell$ follows an equipotential contour, and L is the length of the contour. While any flux surface can cause topological trapping, LTBs possess a local maximum in $|b^{2\mathrm{D}}|^2_{\mathrm{av}}$, which is related to the suppression of slab diffusion, so they define flux surfaces that field lines cross with particular difficulty. As such, they are likely to coincide with sharp gradients in the density of field lines connected to the source, i.e., dropout features. LTBs were indeed found to play this role in simulations using random-phase 2D+slab magnetic fields (Chuychai et al. 2007). The present work examines whether they still serve as good indicators of dropout features when using more physically realistic 2D MHD fields, or whether intense field regions or current sheets provide better indicators.

We find LTBs by the following procedure. We begin with the results of the 2D MHD procedure for the magnetic potential $a(x,y)$ at each to 1024×1024 grid points, and trace contours of constant potential. We consider square cells between grid points, and the cell boundaries are lines between neighboring grid points. Values of a are stepped upward or downward from zero with a constant spacing of 0.05 in units of $B_0\lambda$. For a given value of a, the tracing of equipotential contours uses linear interpolation along the cell boundary to find where contours exit and enter each 2D cell. For simplicity, contour segments within a cell are taken to be straight lines. When there are two entrance points and two exit points for the same cell, the pairing of entrance and exit points is based on the values of a at the four surrounding grid points, in a manner consistent with bilinear interpolation of a within the cell. Segments in adjacent cells are then linked to form closed contours. (When identifying the boundaries of the simulation region with periodic boundary conditions, there are no open contours.)

For each contour, the integration in Equation (11) is approximated by summing over segments within cells, taking the integral along each segment to be represented by $|b^{2\mathrm{D}}|^2$ at the segment center times the segment length. We plot $|b^{2\mathrm{D}}|^2_{\mathrm{av}}$ for each contour line, and visually compare these values between neighboring contours. Contours that have a maximal value compared with neighboring contours are identified as LTBs.

3. RESULTS AND DISCUSSION

3.1. Characteristics of the 2D MHD Field

Figure 1 shows an example of the effects of the 2D MHD procedure. Figure 1(a) shows contours of equal potential $a(x, y)$ for a 2D random-phase field. When adding the mean field $B_0\hat{\mathbf{z}}$, the combined magnetic field twists along flux surfaces defined by the contours of constant a. This 2D random-phase field was used as the initial configuration for a 2D MHD procedure, and Figure 1(b) shows the equipotential contours for the resulting 2D MHD field. While the larger-scale turbulent features remain similar, the most obvious difference is that the random-phase contours are more irregular. These are smoothed in the 2D MHD field because irregularities in magnetic pressure are relieved by the fluid flow, tending to produce a smoother field magnitude $|\mathbf{b}|$. This is consistent with previous findings that MHD turbulence leads to the formation of many flux tubes, which relax locally at every stage of evolution while interacting with one another at their boundaries (Servidio et al. 2008). A related effect is that for this 2D MHD field, the spacing between contours, which indicates $|\mathbf{b}|$, is more uniform in many places.

Nevertheless, some variations in b^2 remain in the 2D MHD model, as shown in Figure 1(c). Note the tendency of regions with strong b^2 to be somewhat aligned with the equipotential contours. This is not particular to the 2D MHD procedure, but is rather related to the solenoidal property $\nabla \cdot \mathbf{b} = 0$, or in Fourier space, $\mathbf{k} \cdot \mathbf{b} = 0$. Variations in the field are also indicated by the current $\mathbf{j}$. For the 2D MHD field, as discussed earlier, the current can be highly concentrated in narrow current cores and current sheets (Figure 1(d)). We will discuss these in more detail shortly.

A comparison of the power spectra of the 2D random-phase and 2D MHD models is presented in Figure 2. Here, we plot the omnidirectional power spectra, $\mathcal{E}(k_\perp)$, as estimated from $|b_x^{2\mathrm{D}}|^2 + |b_y^{2\mathrm{D}}|^2$ summed over Fourier modes in all directions with $k_\perp$ near the value of interest. Both spectra are normalized to the same energy $\langle b^2\rangle^{2\mathrm{D}}$, which is the integral of the power spectrum, and magnetic fields are expressed in units of B_0. By construction, the 2D random-phase model has a power spectrum that rises with $k_\perp$ in the energy-containing range (at low $k_\perp$) and obeys the Kolmogorov law $\mathcal{E} \propto k^{-5/3}$ in an inertial range at higher $k_\perp$. The rollover at and above $k_\perp \approx 4000$ is an artifact of the limited extent of the FFT grid in some directions in $\mathbf{k}$-space. The 2D MHD spectrum is steeper at high $k_\perp$ than the 2D random-phase spectrum. This is a manifestation of the decay of turbulence due to MHD dissipation and the absence of energy input (driving). Note that the turbulent cascade proceeds faster for higher $k_\perp$, and the 2D MHD simulation is run for a fixed time duration, so only the high-$k_\perp$ portion of the spectrum is significantly eroded by the turbulent cascade. More generally, a spectrum that steepens with increasing $k_\perp$ is associated with intermittency, which in this case is associated with decaying turbulence but could also be associated with steady-state dissipation or other effects (Frisch 1995, p.139). Because of the overall normalization, the 2D MHD

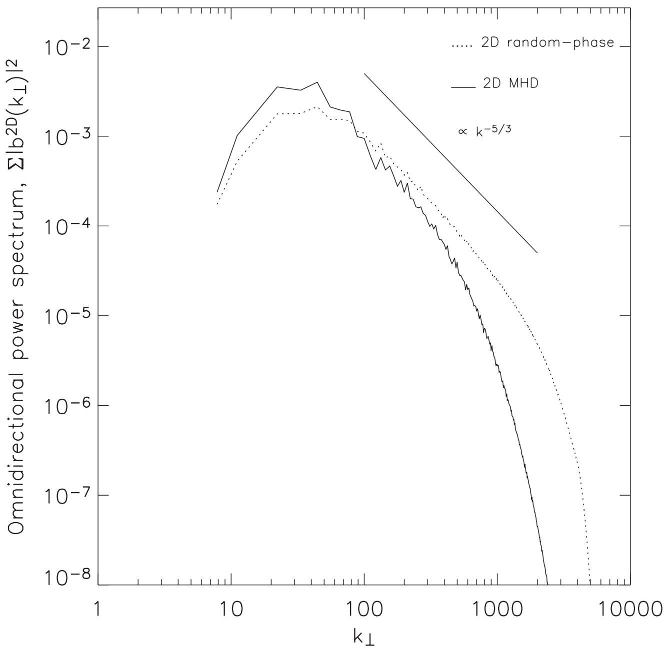

Figure 2. Omnidirectional power spectra of 2D random-phase and 2D MHD turbulent magnetic field models, normalized to the same total energy. After the fixed-time 2D MHD procedure, the high-wavenumber portion of the spectrum has been eroded by the turbulent cascade, which affects the overall normalization.

spectrum at low $k_\perp$ becomes higher than the 2D random-phase spectrum.

Figure 3 shows surface plots of various quantities for the 2D random-phase and 2D MHD models; the vertical scales are for magnetic fields in units of B_0 and lengths in units of λ. In the 2D random-phase models, many wave modes are superimposed with appropriate amplitudes but random phases. This leads to random, irregular structures. It is seen that the magnetic potential, $a(x, y)$, is much smoother in the 2D MHD model because of the tendency of magnetic pressure to smooth variations in b^2. Similarly, the 2D MHD magnetic energy b^2 is seen to typically vary less sharply (over longer distance scales) than the 2D random-phase magnetic energy.

Variations in the magnetic field can be expressed in terms of the current, $\mathbf{j} = \nabla \times \mathbf{b}$, which for the 2D fields is exactly along the z-direction, so we will simply use j to refer to the z-component. The 2D MHD procedure follows the scalar magnetic potential a in Fourier space, and the current density is computed algebraically in $\mathbf{k}$-space. For the 2D random-phase field, we infer the current in the spatial domain by finite differencing, which we call j_{FD}.

For comparison purposes, Figures 3(e) and (f) show j_{FD} in real space, for both fields. In most locations, the current is greatly reduced in the 2D MHD model because of the tendency to smooth variations in the field magnitude. This is related to rapid relaxation and suppression of nonlinearity at most locations (Servidio et al. 2008). However, insofar as the 2D MHD procedure is not continued long enough for all magnetic fields to reconnect and change topology completely, strong persistent current features are generated in association with islands and at certain topological defects. These can be identified as current cores or current sheets (see Figure 2 of Kittinaradorn et al. 2009; see also Greco et al. 2009). At these particular locations, the nonlinearity may be very strong even though it is suppressed in the global average (Servidio et al. 2008). Current cores are found at O-points, i.e., maxima or minima in the potential, where the magnetic field goes to zero; this is a topological defect where the magnetic pressure b^2 cannot be uniform. In the flux tube view, current cores are at the centers of flux tubes. Current sheets are typically found at X-points, i.e., saddle points in the potential, where the field again goes to zero. In particular, when two regions of plasma with oppositely directed magnetic fields flow toward each other, the magnetic field lines can reconnect in a thin boundary region (Sweet 1958; Parker 1963a; Petschek 1964). Such sharp, localized changes in $\mathbf{b}$ correspond to the strongest currents in the 2D MHD model, dominating the visual features in Figures 1(d) and 3(f).

Note that a view of distinct, independent flux tubes with sharp boundaries would seem to require a sharp change in $\mathbf{b}$ and a strong current j all around the flux tube boundaries. However, in our 2D MHD results, the current sheets are found to be quite localized, encompassing only a small fraction of a flux surface (see Figure 1(d)), which is physically reasonable given the attraction of parallel current structures. This is also a feature of modern models and simulations of magnetic reconnection (Priest & Forbes 2000). In the 2D MHD model, one could say that neighboring flux tube structures are coordinated to arrange a concentration of current in current sheets of limited extent, which to some extent contradicts the view of independent flux tubes with sharp boundaries. Furthermore, if the boundary of a "flux tube" is defined as a flux surface that includes a current sheet, one can have concentric flux tube boundaries, and boundaries that along most of their surface have no sharp field gradients.

The results shown in Figure 3 are consistent with the scenario described by Matthaeus & Montgomery (1980). 2D MHD exhibits a dual cascade of magnetic excitation to larger scales (at lower wavenumbers) and current density to smaller-scale, coherent structures (at higher wavenumbers). Such phase coherence of Fourier modes cannot be obtained in random-phase models.

It is interesting to quantitatively confirm that the 2D random-phase and 2D MHD models have different statistical distributions of quantities related to the magnetic field. For the simulated distributions of magnetic potential, magnetic field, and current, we have determined the fourth moment (sometimes called "kurtosis" or "flatness") and, as a check, the sixth moment as well (Table 1). The fourth moment is divided by the variance squared to yield a dimensionless quantity, which would be 3 for a Gaussian distribution. Similarly, the sixth moment is divided by the variance cubed, which would be 15 for a Gaussian distribution. For a distribution with weaker tails than a Gaussian, the normalized fourth and sixth moments would be lower than 3 and 15, respectively, and for a distribution with stronger tails they would be higher. The uncertainty of our determination can be estimated by comparing values for b_x and b_y for all models. These should be the same because the models are axisymmetric. From these, we estimate uncertainties of about 0.08 and 1.19 for the fourth and sixth moments, respectively.

In Table 1, for the slab and 2D random-phase fields, all the quantities have fourth and sixth moments that are consistent with Gaussian values. This is perhaps not surprising because random-phase quantities represent the superposition of a large number of independent Fourier modes, so the resulting quantity should have a Gaussian distribution by the central limit theorem. On the other hand, some quantities in the 2D MHD model are significantly different from Gaussian values. The distribution of potential values is still consistent with a Gaussian distribution,

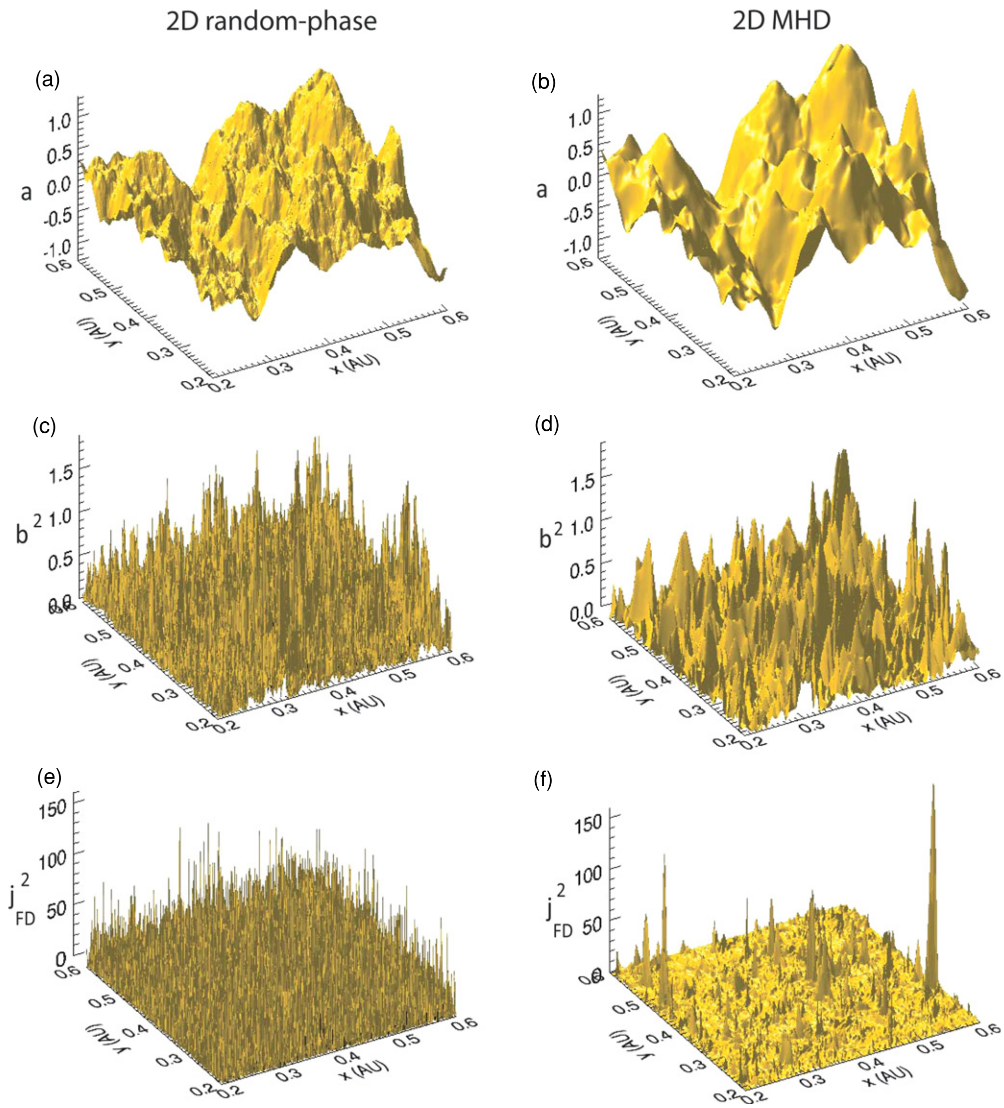

Figure 3. Comparison of quantities pertaining to two models of 2D magnetic turbulence, 2D random-phase (left panels) and 2D MHD (right panels): (a, b) Magnetic potential, a. (c, d) Magnetic energy, b^2. (e, f) j_{FD}^2, where the current $\mathbf{j}_{2D}$ is determined from finite differencing of $\mathbf{b}$. In the more physical 2D MHD model, a is smoother, b varies more gradually, and j is concentrated in narrow current sheets.

Table 1
Moments of Various Quantities for Magnetic Field Models

Model	Quantity	Fourth Moment[a]	Sixth Moment[b]
Slab random-phase	b_x	3.02	15.43
	b_y	2.95	14.36
2D random-phase	a	3.04	14.51
	b_x	3.06	15.94
	b_y	2.93	13.98
	j_{FD}[c]	3.01	15.18
2D MHD	a	3.04	14.50
	b_x	*2.76*	*12.37*
	b_y	*2.67*	*11.02*
	j_{FD}[c]	*7.65*	*331.28*
	j	*6.80*	*242.05*

Notes.
[a] Normalized to second moment squared, i.e., $\langle b_x^4\rangle/(\langle b_x^2\rangle)^2$. The value would be 3 for a Gaussian distribution. Italics indicate values significantly different from 3.
[b] Normalized to second moment cubed, i.e., $\langle b_x^6\rangle/(\langle b_x^2\rangle)^3$. The value would be 15 for a Gaussian distribution. Italics indicate values significantly different from 15.
[c] FD indicates finite differencing.

perhaps because the main effect of the 2D MHD procedure on a is to smooth small-scale irregularities. However, the magnetic fields have fourth and sixth moments that are significantly lower than Gaussian values, apparently due to the physical process that the magnetic pressure becomes more uniform on small scales. The currents exhibit the strongest deviations from Gaussianity. The reduction of the current in most places but strong concentration in current sheets leads to strongly enhanced non-Gaussian tails in the distribution (see also Wan et al. 2009). While the current j derived from Fourier modes has lower moments than that derived from finite differencing of the field, both have moments that are much higher than Gaussian values. The non-Gaussian 2D MHD distributions of b_x, b_y, and j arise from MHD and can be understood physically, so these are taken to be more physically reasonable than the Gaussian distributions of random-phase fields.

Here, we have characterized the physically attractive features of the 2D MHD model, and in particular how it incorporates elements of the flux tube view. Next, we review the mechanisms that have been identified as underlying dropout features, and consider whether the physically realistic features of 2D MHD simulations should actually affect those mechanisms.

3.2. *Reasons for Dropout Features*

If one accepts that SEP dropout features are associated with the filamentation of magnetic connection to the particle source (Mazur et al. 2000; Giacalone et al. 2000), then the next question is why such filamentation occurs with sharp boundaries, given that uniform field line diffusion over 1 AU would be expected to lead to a substantial spread in magnetic connection (Ruffolo et al. 2003, 2004).

One specific mechanism, developed in the context of the 2D+slab magnetic field model, is topological trapping of field lines along flux surfaces of constant 2D potential $a(x, y)$, with eventual diffusive escape due to the slab fluctuations (Ruffolo et al. 2003). In essence the mean field and 2D field are viewed as the main determinants of field line motion, along such 2D flux surfaces, with slab fluctuations as a perturbation; this approach is justified by the minor (15%–20%) contribution of slab fluctuations to the total fluctuation energy (Bieber et al. 1994, 1996).

An additional mechanism is the suppression of diffusive escape when the 2D field is strong or irregular (Chuychai et al. 2005, 2007). This mechanism has also been demonstrated for particle orbits (Tooprakai et al. 2007). However, the demonstrations of both mechanisms for turbulent fields have so far employed random-phase simulations.

While it is clearly more realistic to use 2D MHD fields in place of 2D random-phase fields, it is not clear whether this will actually influence the mechanisms for dropout features. In the flux tube view, it has been proposed that field lines are confined within small-scale flux tubes (Borovsky 2008; which is indeed largely the case for large-scale flux ropes, e.g., in magnetic clouds). However, in our 2D MHD simulation results, flux tube-like structures are found to have weak variations in magnetic fields across most of their "boundaries." Topological trapping applies to any flux surface, and it is not clear that flux surfaces that contain current sheets over narrow portions should trap field lines more effectively.

According to Chuychai et al. (2007), the flux surfaces that trap field lines most effectively are those with high 2D magnetic energy, a key factor in the suppression of slab diffusive escape, i.e., the LTBs. (The other key factor, the irregularity of the 2D equipotential contour, is not considered in the definition of LTBs, and is indeed less important when using a 2D MHD model where such irregularity is greatly reduced; see Figure 1.) The LTBs are not necessarily found at boundaries of flux tube-like structures. While it is physically more realistic to use a 2D MHD model that allows for current sheets, it is not clear that the current sheets should play a major role in field line trapping, as has been expected in the flux tube view (see also Chollet & Giacalone 2008).

3.3. *Associations with Dropout Features*

The observed lack of a strong association between magnetic field changes (such as current sheets) and dropout features has been expressed as a criticism of explanations of dropouts in terms of turbulence (Chollet & Giacalone 2008), though it actually poses more of a challenge to the flux tube viewpoint. Previous turbulence models expected dropout features to occur along LTBs (see Section 2.5), which encapsulate the two identified mechanisms for field line trapping, but those models did not allow for strong current sheets and are not able to directly address such observations. We note that Mazur et al. (2000) reported a general lack of an association with magnetic or plasma signatures. This can be taken to rule out a strong association between the magnetic field intensity and dropout features, and in the present work, we examine whether turbulence models predict such an association.

Our simulation results for a 2D MHD model, which does allow for current sheets, are shown in Figure 4. Given the mean magnetic field along $\hat{\mathbf{z}}$ and two-component 2D+slab magnetic turbulence, we have traced 10,000 magnetic field lines from initial locations within a circle of radius 0.1 AU. The scatter plots in Figure 4 show (x, y) locations of the same field lines after tracing them for a distance z of 1.0 AU. We also traced trajectories for protons of various energies. Up to $\sim$1 GeV, the maps of where particle and field line trajectories intersect $z = 1$ AU are very similar. (Note that observations of dropouts have typically been for particles below $\sim$1 MeV/nucleon.) Thus, we conclude that the locus of field line trajectories is a good proxy for where the SEPs will travel on their way out from the source. The sharp gradients in the density of points in Figure 4 are locations where a spacecraft traversed by solar wind with such a magnetic structure would observe dropouts.

In Figure 4(a), the scatter plot of field line locations is superimposed with contours of equal potential $a(x, y)$ as in Figure 1(b), for a regular spacing in a. It is clear that the boundaries of field line connectivity are related to the equipotential contours, i.e., 2D flux surfaces. This is evidence for topological trapping (Ruffolo et al. 2003). Though "islands" or flux tube-like structures are clearly seen, from this plot alone, it is not clear what determines the location of dropout features. In several locations, they are clearly not associated with the visual "boundary" of an island (e.g., at the coordinates (0.34,0.43), (0.40,0.50), and (0.47,0.39)).

Figure 4(b) superimposes the scatter plot with LTBs, particular flux surfaces where $|b^{2D}|^2_{av}$ has a maximum for the 2D component (see Equation (11)). In numerous locations (including the specific locations mentioned above), the LTBs correctly identify which flux surfaces serve as boundaries in field line connectivity. Physically, these flux surfaces are particularly difficult for field lines to penetrate because of the suppression of slab diffusion across contours where the 2D field is strong (Chuychai et al. 2005, 2007). In many cases, field lines from the initial source region remain present (or absent) on both sides of an LTB, so not all locations along LTBs are associated with dropouts. Likewise, not all sharp boundaries in field line connectivity are associated with LTBs (they can also be associated with the boundary of the initial source region, as deformed by the mapping to 1 AU), but on the whole there is a reasonably good association.

Note that LTBs are often concentric, and thus do not serve as proper boundaries of islands or flux tubes. They are quite specific to field line connectivity and related phenomena such as dropouts. They are not space filling, in the sense that some field lines can travel out from the injection region without having to cross an LTB. This is an important requirement for consistency with the high rate of diffusion observed over long timescales (Kaghashvili et al. 2006).

We also examine whether the simulation results indicate an association with strong turbulent magnetic fields. Such an association has not been obvious in observations (Mazur et al. 2000). Here, we specifically examine an association with $|b^{2D}|^2$ (Figure 4(c)). In the simulation results, there is a degree of association, notably near the coordinates (0.34,0.43), but it is substantially weaker than the association with LTBs. The

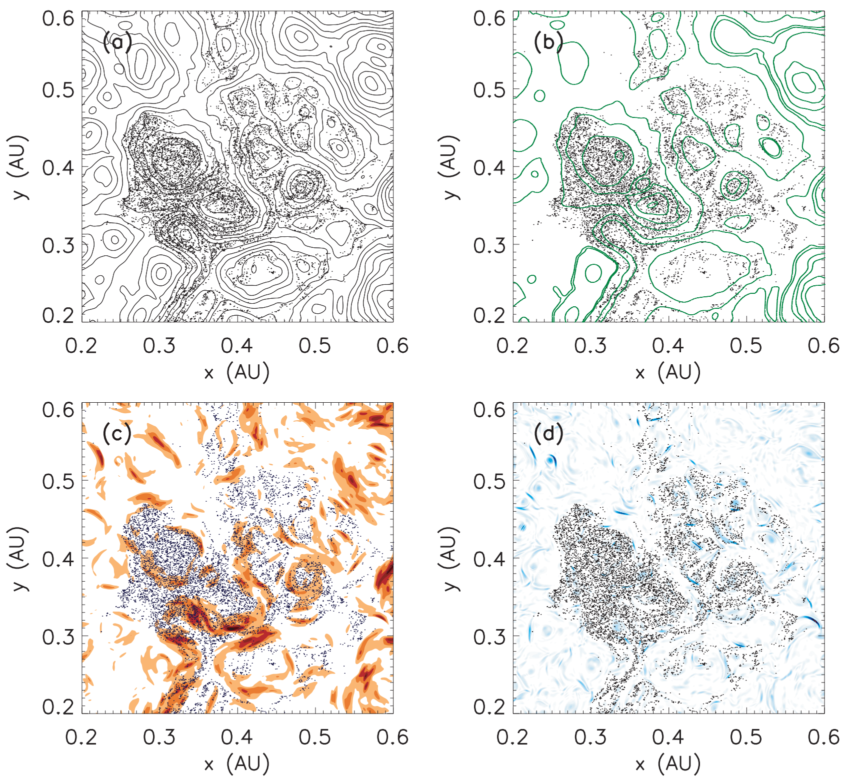

Figure 4. For a mean magnetic field along $\hat{\mathbf{z}}$ and two-component magnetic turbulence, we trace 10,000 magnetic field lines from initial locations within a circle of radius 0.1 AU. These scatter plots show $(x,\ y)$ locations of field lines after a distance z of 1.0 AU, superimposed with indications of (a) contours of constant potential $a(x,y)$ at equal intervals Δa, (b) LTBs (contours; green), (c) b^2 (red), and (d) j^2 (blue). Sharp gradients in magnetic connection to the source, i.e., dropout features, are seen to be associated frequently with LTBs, sometimes with large b^2, and infrequently with current sheets.

reason is that topological trapping naturally occurs along an entire flux surface, whereas only some portions of an LTB have high 2D fields. In spacecraft observations, variations in the 2D field strength are not readily isolated from other magnetic field fluctuations. Thus, a moderate degree of association between dropout features and $|b^{2D}|^2$ may be difficult to observe in the interplanetary medium, where there are independently varying slab fluctuations, and the mean field itself varies over large scales.

Finally, Figure 4(d) shows that dropout features are typically not associated with the current sheets in this model. Thus, the observed lack of association between dropouts and current sheets or sharp magnetic field changes should not be construed as in conflict with turbulence models.

It is perhaps vexing that the physical mechanisms for field line trapping result in a better association with LTBs, which are mathematical constructs and difficult to identify in magnetic field observations along a one-dimensional spacecraft trajectory, than with current sheets, which are relatively easy to identify. However, nature is not obliged to provide easy diagnostics.

4. CONCLUSIONS

Recent theoretical progress to explain SEP dropouts has identified mechanisms for sharp changes in field line connection from a source to an observing region at a distance of 1 AU, in the context of random-phase turbulence models. A viewpoint involving "spaghetti" of independent flux tubes has also been proposed to explain various discontinuities in solar wind plasma properties.

Here, we improve a random-phase turbulence model by using a 2D MHD procedure. The 2D MHD model contains narrow current sheets and structures reminiscent of flux tubes, with non-Gaussian statistics for **b** and **j**. To the extent that flux tubes can be defined, they are not independent but rather coordinated with their neighbors to avoid strong changes in magnetic field along their boundaries, except at current sheets of narrow extent.

Our simulations indicate that magnetic field line trajectories to 1 AU serve as good proxies for arrival locations of protons up to 1 GeV in energy. Thus, sharp changes in magnetic connection to a localized source are a proxy for SEP dropout features. We identified LTBs as 2D flux surfaces with maximal $|b^{2D}|^2_{av}$ compared with neighboring flux surfaces. Our simulation results indicate that dropout features are frequently associated with LTBs, sometimes associated with strong 2D magnetic fluctuations, and only infrequently associated with current sheets. The mechanisms identified in the context of random-phase two-component fields can still explain dropout features with the 2D MHD model. In sum, we have developed a more realistic model of turbulent fluctuations in the solar wind, including current sheets, which is consistent with the poor observed association between dropout features and intense magnetic fields or currents.

The authors thank Rakpong Kittinaradorn for technical assistance. This work was supported by the Thailand Research Fund, NASA grant NNG05GG83G, the NASA Heliophysics Theory program, NASA NNX08AI47G, and the SHINE program, NSF ATM0752135.

REFERENCES

Bieber, J. W., Matthaeus, W. H., Smith, C. W., Wanner, W., Kallenrode, M.-B., & Wibberenz, G. 1994, ApJ, 420, 294

Bieber, J. W., Wanner, W., & Matthaeus, W. H. 1996, J. Geophys. Res., 101, 2511
Borovsky, J. E. 2008, J. Geophys. Res., 113, A08110
Bruno, R., Carbone, V., Veltri, P., Pietropaolo, E., & Bavassano, B. 2001, Planet. Space Sci., 49, 1201
Cane, H. V., & Erickson, W. C. 2003, J. Geophys. Res., 108, 1203
Cane, H. V., Wibberenz, G., Richardson, I. G., & von Rosenvinge, T. T. 1999, Geophys. Res. Lett., 26, 565
Chollet, E. E., & Giacalone, J. 2008, ApJ, 688, 1368
Chuychai, P., Ruffolo, D., Matthaeus, W. H., & Meechai, J. 2007, ApJ, 659, 1761
Chuychai, P., Ruffolo, D., Matthaeus, W. H., & Rowlands, G. 2005, ApJ, 633, L49
Coleman, P. J. 1968, ApJ, 153, 371
Dasso, S., Milano, L. J., Matthaeus, W. H., & Smith, C. W. 2005, ApJ, 635, L181
Frisch, U. 1995, Turbulence: The Legacy of A. N. Kolmogorov (Cambridge: Cambridge Univ. Press)
Giacalone, J., Jokipii, J. R., & Matthaeus, W. H. 2006, ApJ, 641, L61
Giacalone, J., Jokipii, J. R., & Mazur, J. E. 2000, ApJ, 532, L75
Goldreich, P., & Sridhar, S. 1995, ApJ, 438, 763
Gosling, J. T., Skoug, R. M., McComas, D. J., & Mazur, J. E. 2004, ApJ, 614, 412
Greco, A., Matthaeus, W. H., Servidio, S., Chuychai, P., & Dmitruk, P. 2009, ApJ, 691, L111
Higdon, J. C. 1984, ApJ, 285, 109
Hossain, M., Gray, P. C., Pontius, D. H., Matthaeus, W. H., & Oughton, S. 1996, in AIP Conf. Proc. 382, Solar Wind Eight, ed. D. Winterhalter, J. T. Gosling, S. R. Habbal, W. S. Kurth, & M. Neugebauer (Woodbury, NY: AIP), 81
Jokipii, J. R., & Coleman, P. J. 1968, J. Geophys. Res., 73, 5495
Jokipii, J. R., & Parker, E. N. 1968, Phys. Rev. Lett., 21, 44
Kaghashvili, E. Kh., Zank, G. P., & Webb, G. M. 2006, ApJ, 636, 1145
Kittinaradorn, R., Ruffolo, D., & Matthaeus, W. H. 2009, ApJ, 702, L138
Kolmogorov, A. N. 1941, Akad. Nauk SSSR Dokl., 30, 301
Leamon, R. J., Smith, C. W., Ness, N. F., Matthaeus, W. H., & Wong, H. K. 1998, J. Geophys. Res., 103, 4775
Li, G. 2008, ApJ, 672, L65
Matthaeus, W. H., Bieber, J. W., Ruffolo, D., Chuychai, P., & Minnie, J. 2007, ApJ, 667, 956
Matthaeus, W. H., Goldstein, M. L., & Roberts, D. A. 1990, J. Geophys. Res., 95, 20673
Matthaeus, W. H., Gray, P. C., Pontius, D. H., Jr., & Bieber, J. W. 1995, Phys. Rev. Lett., 75, 2136
Matthaeus, W. H., & Lamkin, S. L. 1986, Phys. Fluids, 29, 2513
Matthaeus, W. H., & Montgomery, D. C. 1980, Ann. New York Acad. Sci., 357, 203
Matthaeus, W. H., Smith, C. W., & Oughton, S. 1998, J. Geophys. Res., 103, 6495
Matthaeus, W. H., Zank, G. P., & Oughton, S. 1996, J. Plasma Phys., 56, 659
Mazur, J. E., Mason, G. M., Dwyer, J. R., Giacalone, J., Jokipii, J. R., & Stone, E. C. 2000, ApJ, 532, L79
McCracken, K. G., & Ness, N. F. 1966, J. Geophys. Res., 71, 3155
McKibben, R. B. 2005, Adv. Space Res., 35, 518
McKibben, R. B., Lopate, C., & Zhang, M. 2001, Space Sci. Rev., 20, 257
Montgomery, D. 1982, Phys. Scr., T2, 83
Moraal, H. 1976, Space Sci. Rev., 19, 845
Osman, K. T., & Horbury, T. S. 2007, ApJ, 654, L103
Oughton, S., Priest, E. R., & Matthaeus, W. H. 1994, J. Fluid Mech., 280, 95
Parker, E. N. 1963a, ApJS, 8, 177
Parker, E. N. 1963b, Interplanetary Dynamical Processes (New York: Wiley Interscience)
Parker, E. N. 1965, Planet. Space Sci., 13, 9
Petschek, H. E. 1964, in The Physics of Solar Flares, ed. W. N. Hess (NASA SP-50; Washington, DC: NASA), 425
Pommois, P., Zimbardo, G., & Veltri, P. 2005, Adv. Space Res., 35, 647
Press, W. H., Teukolsky, S. A., Vetterling, W. T., & Flannery, B. P. 1992, Numerical Recipes in FORTRAN: The Art of Scientific Computing (2nd ed.; Cambridge: Cambridge Univ. Press)
Priest, E. R., & Forbes, T. 2000, in Magnetic Reconnection: MHD Theory and Applications, (Cambridge: Cambridge Univ. Press)
Reames, D. V. 1992, in IAU Colloq. 133, Eruptive Solar Flares, ed. Z. Švestka, B. V. Jackson, & M. E. Machado (Lecture Notes in Physics, Vol. 399; Berlin: Springer), 180
Reames, D. V., Cane, H. V., & von Rosenvinge, T. T. 1990, ApJ, 357, 259
Reinecke, J. P. L., McDonald, F. B., & Moraal, H. 2000, J. Geophys. Res., 105, 27439
Ruffolo, D., Matthaeus, W. H., & Chuychai, P. 2003, ApJ, 597, L169
Ruffolo, D., Matthaeus, W. H., & Chuychai, P. 2004, ApJ, 614, 420
Sahraoui, F., Goldstein, M. L., Robert, P., & Khotyaintsev, Y. V. 2009, Phys. Rev. Lett., 102, 231102
Saur, J., & Bieber, J. W. 1999, J. Geophys. Res., 104, 9975
Servidio, S., Matthaeus, W. H., & Dmitruk, P. 2008, Phys. Rev. Lett., 100, 095005
Shalchi, A., Bieber, J. W., & Matthaeus, W. H. 2008, A&A, 483, 371
Shebalin, J. V., Matthaeus, W. H., & Montgomery, D. 1983, J. Plasma Phys., 29, 525
Smith, C. W., Matthaeus, W. H., Zank, G. P., Ness, N. F., Oughton, S., & Richardson, J. D. 2001, J. Geophys. Res., 106, 8253
Strauss, H. 1976, Phys. Fluids, 19, 134
Sweet, P. A. 1958, in IAU Symp. 6, Electromagnetic Phenomena in Cosmic Physics, ed. B. Lehnert (New York: Cambridge Univ. Press), 123
Tooprakai, P., Chuychai, P., Minnie, J., Ruffolo, D., Bieber, J. W., & Matthaeus, W. H. 2007, Geophys. Res. Lett., 34, L17105
Verma, M. K., Roberts, D. A., & Goldstein, M. L. 1995, J. Geophys. Res., 100, 19839
von Kármán, T., & Howarth, L. 1938, Proc. R. Soc. Lond. A, 164, 192
Wan, M., Oughton, S., Servidio, S., & Matthaeus, W. H. 2009, Phys. Plasmas, 16, 080703
Weygand, J. M., Matthaeus, W. H., Dasso, S., Kivelson, M. G., Kistler, L. M., & Mouikis, C. 2009, J. Geophys. Res., 114, A07213
Zank, G. P., & Matthaeus, W. H. 1991, Phys. Fluids, 3, 69
Zimbardo, G., Pommois, P., & Veltri, P. 2004, J. Geophys. Res., 109, A02113